Interreg Aurora

Co-funded by the European Union

Fraunhofer IWS

FRAUNHOFER-INSTITUT FÜR WERKSTOFF- UND STRAHLTECHNIK IWS

FINAL REPORT

STUDY ON ADDITIVE MANUFACTURING OF HYBRID TEST SPECIMEN USING COAXQUATTRO

ON BEHALF OF

Executive Director
Prof. Dr. Christoph Leyens

Project Manager
Jacob-Florian Mätje

Co-Worker
Mirko Riede
Mark Kaubisch

Fraunhofer-Institut für Werkstoff- und Strahltechnik IWS
Dresden

Project number: 062/
Running time: 12/2023 – 06/2024
Reporting period: 12/2023 – 06/2024

Content

1 Introduction

1.1 Objective of the project

The aim of this project is the additive manufacturing of specimens for mechanical testing by means of novel COAXquattro utilizing a 4-wire feed simultaneously in a hybrid manner. The samples will be produced using three different materials – highly alloyed steel, low alloyed steel and copper alloy. The results of the project shall be a baseline for a benchmark of laser based Direct Energy Deposition (L-DED) and Wire Arc Additive Manufacturing (WAAM).

1.2 Planned Work packages

WP1: Management and communication
Work contents:
- internal and external communication (highly appreciated)

WP2: Setup and preparation
Work contents:
- procurement of required materials
- system setup (Spot 12,5 mm) including monitoring
- calibration of material feed using a quadruple feeder
- detailed specification of test specimen geometries tailored to customer requirements

WP3: Preliminary study
Work contents:
- characterization of the wire by cross sections
- study on processing of each singular alloy in an iterative manner supported by metallographic cross sections to identify robust parameter sets
- if applicable, system adaptions to counteract potential issues e. g. back reflection or thermal load
- study processing on the interface of the named materials using the steel alloy as a substrate and applying the copper alloy aiming low dilution and few defects

WP4: Manufacture of test specimen
Work contents:
- high performance fabrication of minimum 5 test specimen in a hybrid manner – Appling steel in the lower half and copper alloy in the upper half

1.3 Summary

2
Setup and preparation

2.1
Selection and procurement of required materials

2.1.1 Highly alloyed steel

1.4430 also known as ER 316 L Si was chosen because of its wide spread use, good weldability and existing experience with the material using the COAXquattro process head. ER 316 L Si is an austenitic chrome-nickel-molybdenum-steel with increased silicone content developed for MIG and MAG welding and is certified by TÜV, DB and CE. Table 1 shows the chemical composition and selected properties as stated by the manufacturer. Entries marked with * are supplemented from another source.

Fe	C	Si	Mn	Cr	Ni	Mo
base	0.03	0.65-1.2	1.0-2.50	18.0-20,0	11.0-14.0	2.5-3.0

Table 1: Directional analysis of ER 316 L Si feedstock and properties of welded material from manufacturer data sheet

Yield strength [MPa]	Tensile strength [MPa]	Elongation at break %	Impact work [J] (20°C) *	Thermal conductivity [W/(m*K)] *
295	510	25	100	15

4 wire spools of 15 kg each with a wire diameter of 1.6 mm were procured from “METAL TECHNOLOGY CANTERBO GMBH” through one of their resellers.

2.1.2 Low alloyed steel

1.5125 also known as SG2 or G3Si was chosen because of its good weldability, low alloy content and its widespread application. G3Si is a low alloyed, copper plated steel developed for MAG joint welding of low alloyed steels and is certified by TÜV, DB and CE. Table 2 shows the chemical composition and selected properties as stated by the manufacturer. Entries marked with * are supplemented from another source.

Fe	C	Si	Mn	P	S	Cu
base	0.06-0.11	0.8-1.0	1.45-1.55	<0.025	<0.025	<0.30

Table 2: Directional analysis and properties of G3Si feedstock from the manufacturer data sheet

Yield strength [MPa]	Tensile strength [MPa]	Elongation at break %	Impact work [J] (20°C)	Thermal conductivity [W/(m*K)] *
440	550	26	85	35

4 wire spools of 15 kg each with a wire diameter of 1.6 mm were procured from “ELMAG Entwicklungs und Handels GmbH” through one of their resellers.

2.1.3 Copper alloy

2.1461 also known as CuSi-3 was selected due to its low melting point to ensure weldability despite its low absorption coefficient for infrared light and due to its availability as standardized wire feedstock. CuSi-3 is a Copper-Silicon alloy developed for MIG and MAG welding of galvanized steel and is certified by TÜV and CE. Table 3 shows the chemical composition and selected properties as stated by the manufacturer.

Cu	Si	Mn	Sn	Fe
base	2.9	0.9	0.01	0.06

Table 3: Directional analysis and properties of CuSi-3 feedstock from the manufacturer data sheet

Yield strength [MPa]	Tensile strength [MPa]	Elongation at break %	Impact work [J] (20°C)	Thermal conductivity [W/(m*K)]
120	350	40	60	35

4 wire spools of 15 kg each with a wire diameter of 1.6 mm were procured from “ALUNOX Schweißtechnik GmbH” through one of their resellers.

2.1.4 Substrate material

1.0037 also known as S235JR+C was chosen as the substrate material due to low cost, availability and sufficient weldability. S235JR+C is a simple, unalloyed construction steel.

Fe	C	Mn	P	S	Cu	N
base	<0.17	<1.4	<0.04	<0.04	<0.055	<0,012

Table 4: Chemical composition and mechanical properties of S25JR+C according to DIN 10277

Yield strength [MPa]	Tensile strength [MPa]	Elongation at break %
>260	390 - 730	>10%

20 plates with the dimensions of 300x100x25 mm of cold rolled S235JR+C were procured as substrate material from “WIEHLSTAHL Handels GmbH & Co. KG”.

2.2 System setup

The process system comprises several key components, including the COAXquattro (process head), an LDF 20000-200 diode laser by laserline (energy source), a KUKA robot (kinematics), four wire feeders (feedstock supply) and several cameras (process monitoring). The process setup for this study is shown in Figure 2.1.

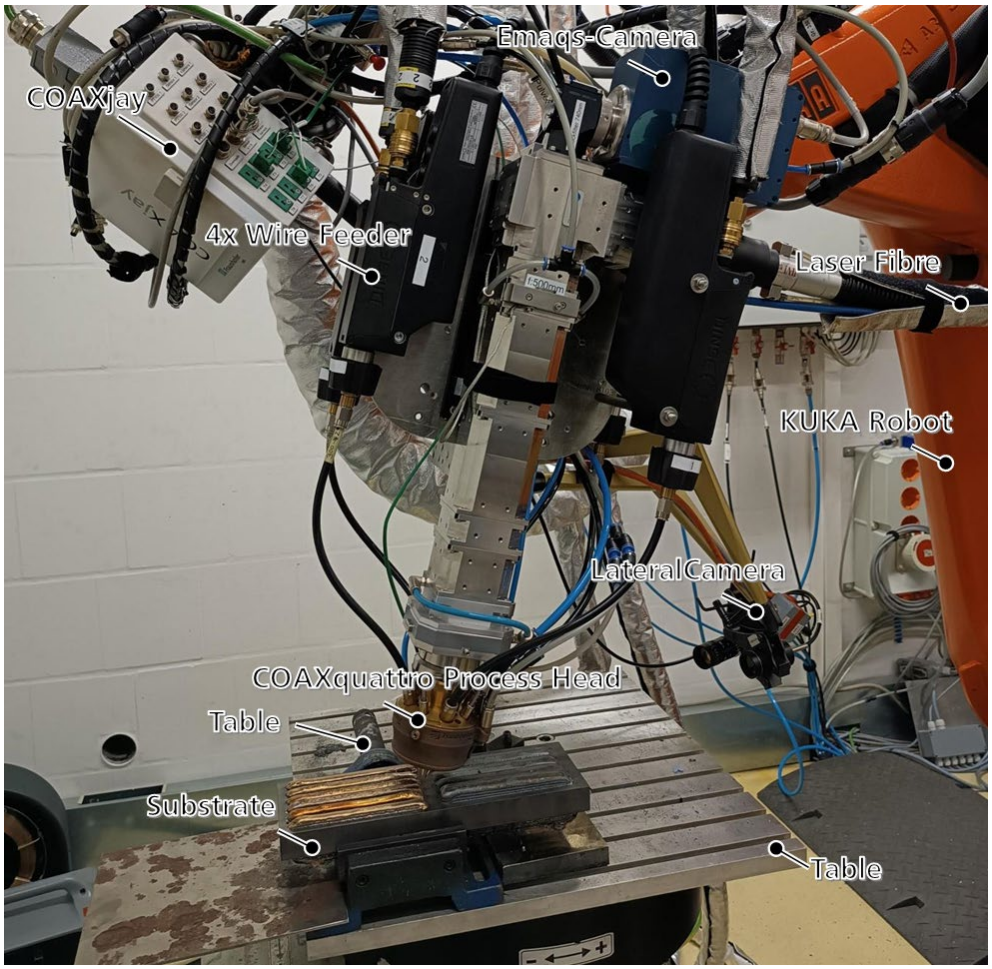

Figure 2.1: Process setup

2.2.1 COAXquattro & Process Monitoring

The high-performance laser welding head COAXquattro is designed for multi-wire deposition with the option of additionally feeding powder at the same time. The laser beam is arranged in the center. The wire or powder feed from the outside. With four separately controllable wires, the nozzle achieves a 100 percent material utilization and high deposition rates. Possible wire diameters range from 0.8 to 1.6 mm. A maximum laser power of 20 kW is focused on a spot between 7 – 12.5 mm in diameter depending on the desired track geometry and deposition rate. An optional inert gas nozzle delivers up to 200l/min of additional shielding gas to protect the melt from oxidation. Figure 2.2 shows a model of the process head with its key components as well as images recorded by the three process monitoring cameras: dome camera (overview), lateral camera (melt pool monitoring) and coaxial camera “Emaqs” (melt pool monitoring).

Figure 2.2: COAXquattro process head and process monitoring

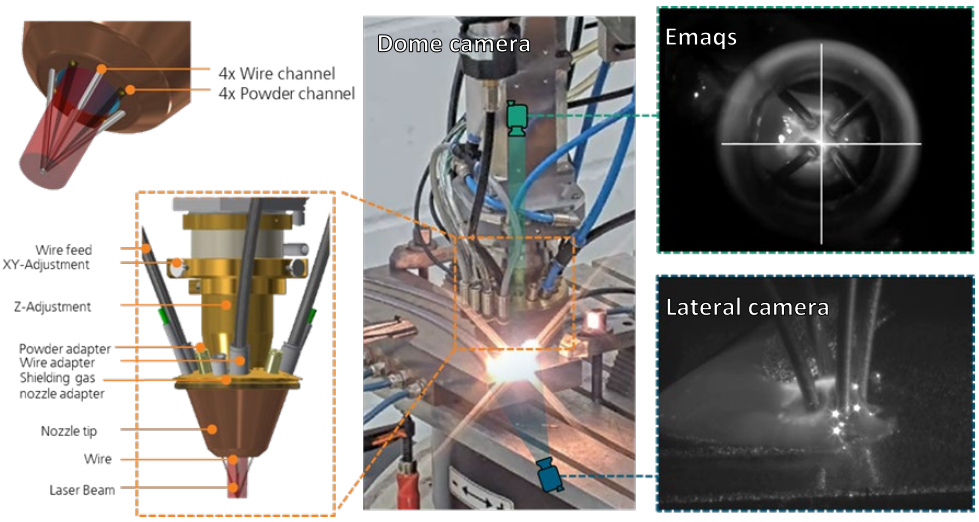

For this study a laser spot size of 12,5 mm was chosen as outlined in Enclosure A of the offer. All feedstock material had a diameter of 1,6 mm to ensure a sufficient mass flow into the large melt pool. The optional inert gas nozzle was installed to keep oxidation as low as possible, resulting in a total Argon flow of 230 l/min during deposition. To counteract back reflection that causes thermal damage to the optical fiber connector the process head is kept at a 15° angle to the normal vector of the substrate material at all times.

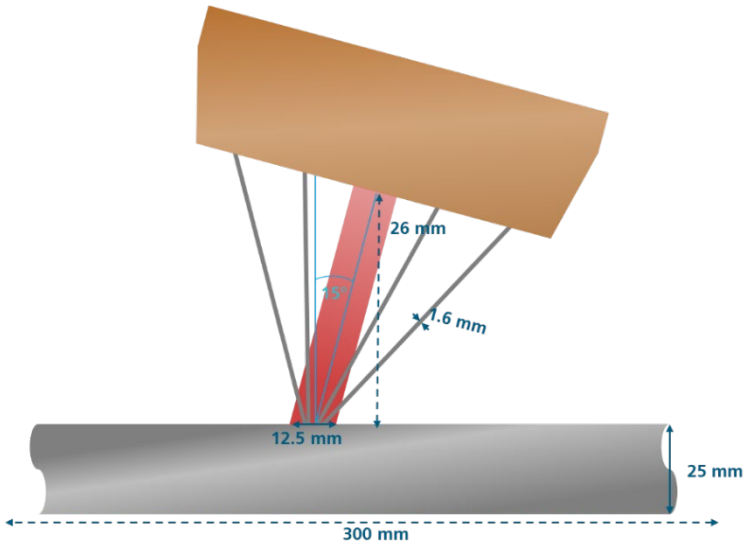

Figure 2.3: Nozzle Configuration and substrate dimensions for this study

Several additional sensors were utilized to monitor the temperature in key positions and the real wire feed rate using the COAXjay system to prevent damage to components and to identify process issues.

2.3 Sample geometry & Configuration

The target sample geometry was chosen as specified by University of Oulu to allow for extraction of specimen for mechanical testing. A sample geometry for the extraction of tensile specimens and a sample geometry for the extraction of fatigue specimens are produced using two different material combinations.

Material combination 1 is composed of ER 316 L Si in the lower half with CuSi-3 comprising the upper half. Material combination *2* is composed of ER 316 L Si in the lower half with *G3Si* comprising the upper half. Figure 2.4 and Figure 2.5 show the required dimensions for tensile and axial fatigue specimen extraction, Figure 2.6 and Figure 2.7 for bending fatigue specimen.

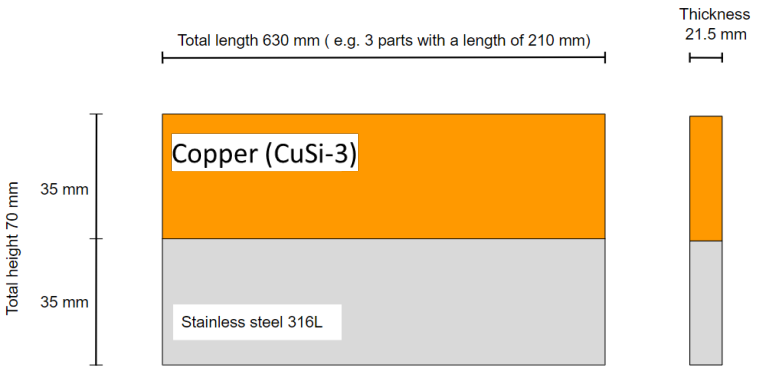

Figure 2.4: Target dimensions and configuration of part type 1, material combination 1

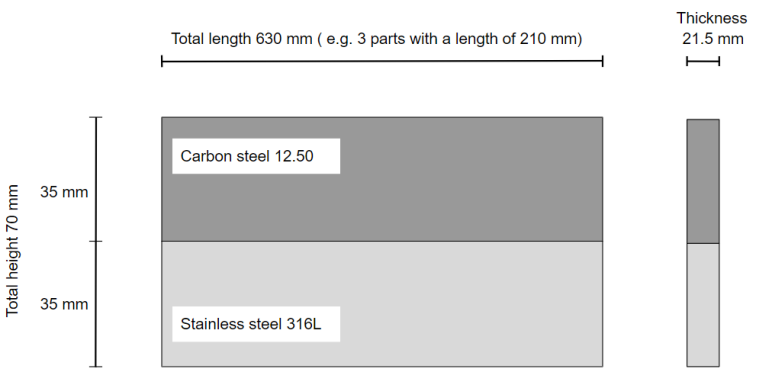

Figure 2.5: Target dimensions and configuration of part type 1, material combination 2

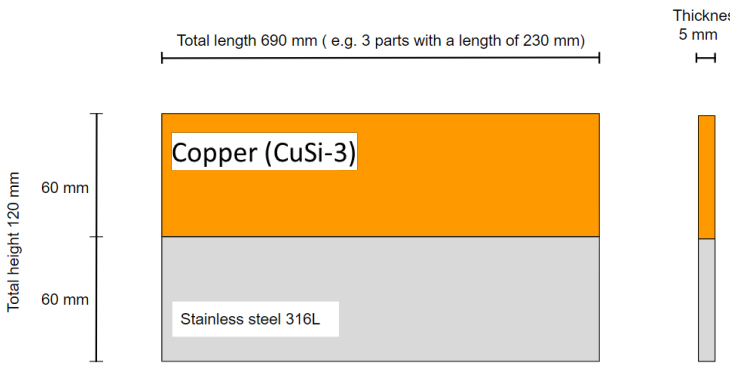

Figure 2.6: Target dimensions and configuration of part type 2, material combination 1

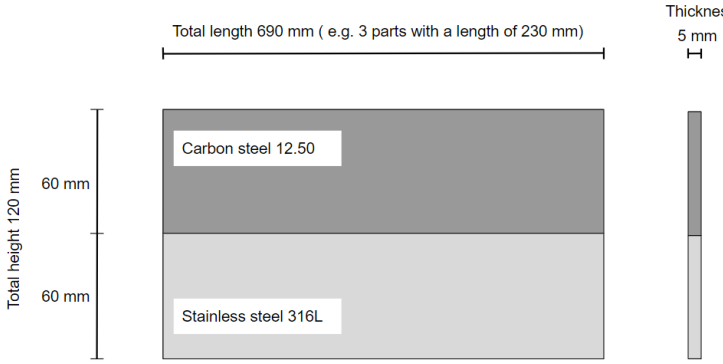

Figure 2.7: Target dimensions and configuration of part type 2, material combination 2

3 Preliminary Study

3.1 Characterization of the wire by cross sections

3.1.1 ER 316LSi

Figure 3.1 shows the metallographic cross section of the ER316LSi wire processed in this study. The polished state shows very little porosity and inclusions. Etching with V2A-Etchant did not reveal the microstructure but preferentially attacked the silicon rich areas resulting in a porous appearance.

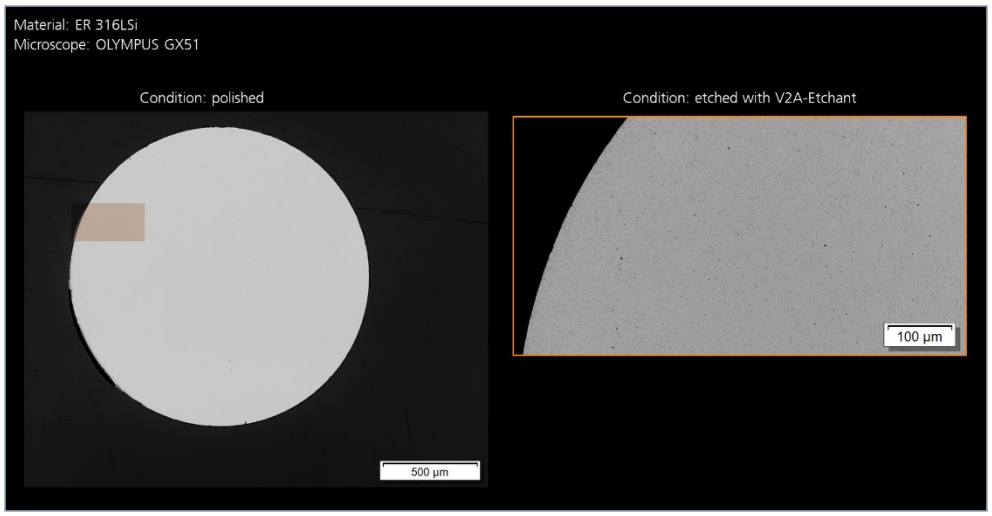

Figure 3.1: Cross section of the ER316LSi wire in different etching states and magnifications

3.1.2 CuSi-3

Figure 3.2 shows the metallographic cross section of the CuSi-3 wire processed in this study. The polished state shows no porosity visible at this magnification. Etching with $(NH_4)_2S_2O_8$ + Adler (10:1) reveals randomly oriented grains and no preferentially attacked areas.

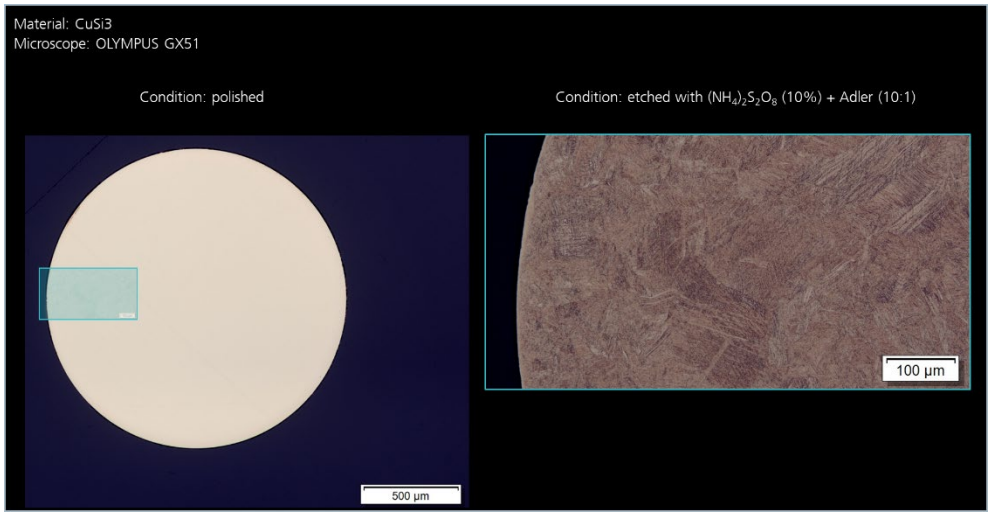

Figure 3.2: Cross section of the CuSi-3 Wire in different etching states and under different magnifications

3.1.3 G3Si

Figure 3.3 shows the metallographic cross section of the G3Si wire processed in this study. The polished state shows only one pore with dimensions over 10 µm. Etching with Nital 2% revealed an α-Ferrite matrix with disperse Fe_3C and Pearlite.

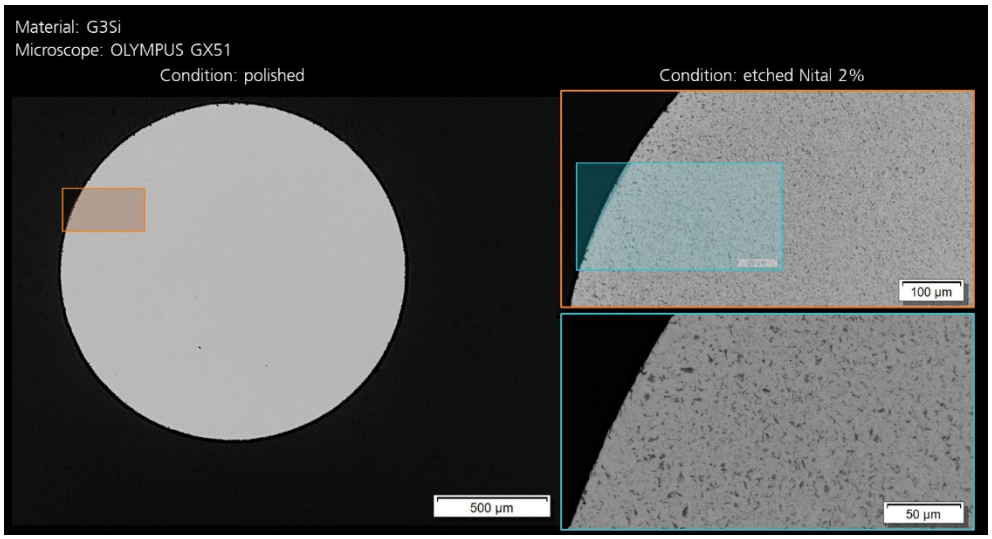

Figure 3.3: Cross section of the G3Si Wire in different etching states and under different magnifications

3.2 Individual Parameter development & process adaptions for the interface

3.2.1 ER 316LSi

In a previous IWS internal study stable process parameters for processing of ER 316 L Si with high deposition rate were investigated for single track walls. The identified parameter space is shown in Table 5.

Parameter	**Range**
Laser power [W]	13000 – 20000
Welding speed [mm/min]	600 – 1200
Wire feed rate [mm/min]	1850 – 4180
Characteristic Value	**Range**
Deposition Rate [kg/h]	7,48 – 16,04
Energy Density [J/mm³]	6,30 – 10,10

Table 5: Parameter Space for ER 316L Si from previous work

Figure 3.4: Single tracks of ER 316L

Si on S235J Substrate

Despite the Argon flow of 230 l/min tracks showed substantial oxidation due to the long melt pool life time and therefore solidification outside the shielded zone. Previous investigations have shown that this oxidation is limited to the surface and does not result in relevant oxide inclusions in the bulk material or between layers.

A short study to adapt these parameters to the sample geometry of part type 1 resulted in the parameter set shown in Table 6.

Parameter	**Value**
Laser power [W]	15500
Welding speed [mm/min]	900
Wire feed rate [mm/min]	2600
Characteristic Value	**Value**
Deposition Rate [kg/h]	9,97
Energy Density [J/mm³]	8,42

Table 6: Stable parameter set for ER 316L Si, part type 1 in this study

3.2.2 CuSi-3

Process development for CuSi-3 was initiated using single tracks and parameters close to those of ER 316LSi and were then iteratively adjusted while transitioning to the geometry of part type 1 on S235JR substrate. The investigated parameter space is shown in Table 7.

Parameter	**Range**
Laser power [W]	15500
Welding speed [mm/min]	600 – 900
Wire feed rate [mm/min]	2000 – 2500
Characteristic Value	**Range**
Deposition Rate [kg/h]	8,20 – 10,25
Energy Density [J/mm³]	8,70 – 13,04

Table 7: Parameter Space investigated for CuSi-3 on S235JR substrate

Figure 3.5: cuboid of CuSi-3 on S235JR Substrate

Depositing the geometry of part type 1 to a height of six Layers on S235JR showed low oxidation and no visible surface cracks. A slight raise of the track end compared to the beginning and middle could also be observed.

Parameter	**Value**
Laser power [W]	15500
Welding speed [mm/min]	675
Wire feed rate [mm/min]	2250
Characteristic Value	**Value**
Deposition Rate [kg/h]	9,23
Energy Density [J/mm³]	11,6

Table 8: Parameter set for cuboid shown in Figure 3.5: cuboid of CuSi-3 on S235JR substrate

Applying the identified process parameters to depositing CuSi-3 on ER 316LSi resulted in severe oxidation and faults, as visible in Figure 3.6.

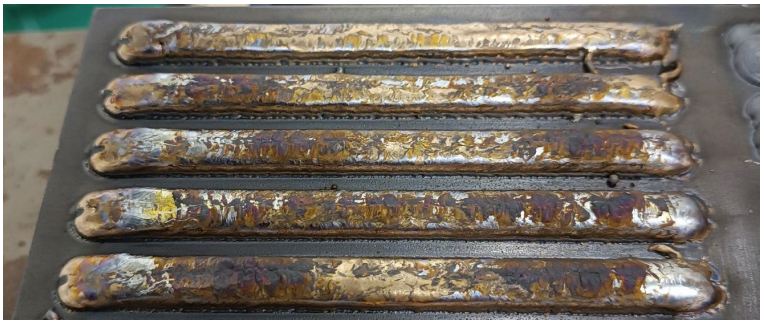

Figure 3.6 CuSi-3 single tracks on ER 316LSi single tracks:

As this was not observed when depositing on S235JR it was assumed that the CuSi-3 reacts with ER 316LSi in a way that negatively impacts the process. Therefore, a parameter study was carried out to try and minimize dilution.

Parameter	**Range**
Laser power [W]	9000 – 15500
Welding speed [mm/min]	600 – 900
Wire feed rate [mm/min]	1510 – 2500

Table 9: Parameter study for CuSi-3 on ER 316LSi

Characteristic Value	Range
Deposition Rate [kg/h]	6,19 – 10,25
Energy Density [J/mm³]	5,05 – 13,04

Figure 3.7: CuSi-3 double tracks on ER 316LSi double tracks, as deposited (left) and steel brushed (right)

However, even with the lowest possible laser power that allows for sufficient melting of the feed stock material with a spot size of 12.5 mm (9000 W), strong oxidation of CuSi-3 persisted. While the oxidation could mostly be removed by steel brush the underlying track showed a highly irregular surface.
As Figure 3.4 shows the ER 316LSi tracks display strong surface oxidation with a slag like appearance. To counteract CuSi-3 interacting with this slag all ER 316LSi surfaces intended for deposition of CuSi-3 were treated with a steel brush from this point on. This only resulted in a marginal increase of the surface quality as too much oxides remained on the ER 316LSi deposits. However, depositing a second layers of CuSi3 on the interface layer showed significantly reduced Oxidation and a smoother surface, as visible in Figure 3.8.

Figure 3.8: Multilayer tracks of CuSi-3 on ER 316LSi

Based on these results the following procedure was implemented for the manufacture of the sample geometry:

1. Sandblasting of the relevant ER 316LSi surfaces
2. Deposition of 1 layer of CuSi-3
3. Steel brushing of CuSi-3 layer
4. Repetition of steps 2 and 3 until CuSi-3 is smooth and oxide free as-built
5. Deposition of layers until required height is reached at all points.

Initial treatment of ER 316LSi was changed to sandblasting for better reproducibility and less remaining oxides. Even though sandblasting could still not fully remove all oxides as visible in Figure 3.9, CuSi-3 layers beyond the first showed progressively lower oxidation and a smoother surface. Geometrical irregularities on the sides are the result of an incorrect working distance in the higher layers. The final parameter set is listed in Table 10.

Parameter	Value
Laser power [W]	13200
Welding speed [mm/min]	900

Table 10: Parameter set for CuSi-3 on ER 316LSi part type 1

Wire feed rate [mm/min]	1780
Characteristic Value	**Value**
Deposition Rate [kg/h]	7.30
Energy Density [J/mm³]	7.41

Figure 3.9: Multilayer CuSi-3 deposition on ER 316LSi part type 1 geometry

3.2.3 G3Si

The process development for G3Si was initiated using the stable parameter set found for ER 316L Si. As stalling of the wires was observed in the lateral process camera and wire feed monitoring, the wire feed rate and welding speed were subsequently reduced until a stable process was achieved. The identified parameter set for the sample geometry of part type 1 is shown in Table 11.

Parameter	**Value**
Laser power [W]	15500
Welding speed [mm/min]	600
Wire feed rate [mm/min]	1600
Characteristic Value	**Value**
Deposition Rate [kg/h]	6,41
Energy Density [J/mm³]	13,04

Table 11: Stable parameter set for G3Si, part type 1 in this study

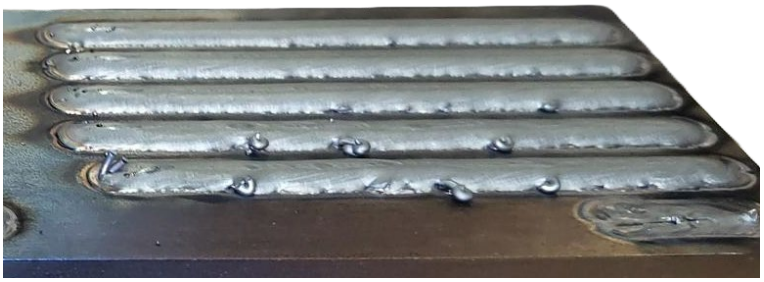

Figure 3.10: single tracks of G3Si on S235JR Substrate

Figure 3.11: cuboid of G3Si on S235JR Substrate

Applying the identified process parameters to depositing G3Si on sandblasted ER 316LSi did not result in any irregular oxidation or surface roughness and could therefore be directly adopted for the manufacture of part type 1, material combination 2 samples.

4 Manufacture of samples

All part type 1 samples were manufactured by employing the same general welding strategy of three overlapping, unidirectional tracks with an overlap around 25%. The welding direction was not changed between layers nor was the order of the individual tracks. This created a predictable geometrical inhomogeneity across the sample with a different expression depending on the material. A variable waiting time was kept between individual tracks and additionally between layers to allow for heat disspation.

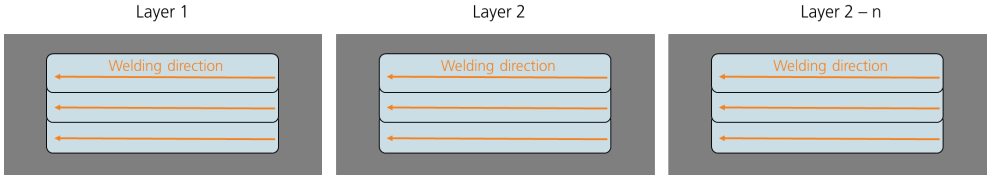

Figure 4.1: Welding strategy for part type 1

4.1 ER 316L Si: part type 1

Manufacture of ER 316L Si: part type 1 samples was carried out using the parameter set listed in Table 6 and the welding strategy shown in Figure 4.1, resulting in a good surface quality on the sides and the previously observed oxidation of the top most layer. For ER 316L Si the combination of unidirectional welding, angled process head, low melt viscosity and heat buildup over the layers resulted an incline towards the track end. With the wire withdrawal process sometimes disrupting the surface tension of the melt pool enough to cause it to flow of the sample. This was deemed acceptable, to reduce manufacturing time, as the substrate dimensions were sufficient to cut the sample at the beginning of the incline and still preserving the target part dimension of 230 mm.

Figure 4.2: Welding strategy for part type 1

4.2 CuSi-3: part type 1

CuSi-3: part type 1 samples were fabricated using the procedure described in section 3.2.2 and the parameters shown in Table 10.

Figure 4.3: Fabrication of CuSi-3: part type 1

Figure 4.4 shows a finished CuSi-3: part 1 sample with visible annealing colors due to heat accumulation. While the CuSi-3 was deposited using the same strategy as ER 316L Si, it shows a very different behavior at the track end. Resulting in an agglomeration of material in that position, that compensated for the missing material in the ER 316L Si part.
Also visible in Figure 4.4 are cracks at the surface of the CuSi-3 part that propagate in build direction and therefore perpendicular to the weld direction. These cracks are likely a result of increasing residual stresses with increasing build height. Continuous observation and photo-documentation of a sample during fabrication showed that these cracks can occur far from the process zone during cooling. No hot cracking was observed.

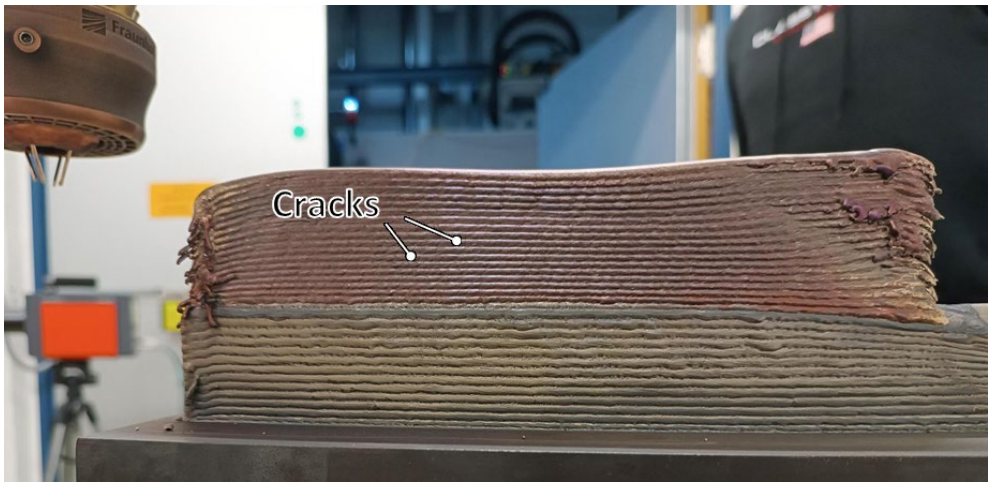

Figure 4.4: Fabricated CuSi-3: part type 1 sample

In an attempt to reduce or suppress one sample was built utilizing a thermal camera to control inter layer temperature (~100°C). This significantly impacted track geometry (Figure 4.5), but only resulted in a slight reduction of visible surface cracks, while heavily impacting

inter layer wait times (>20 minutes). Therefore, the strategy was not adopted for further fabrications due to the resulting very long process times and geometrical inhomogeneity.

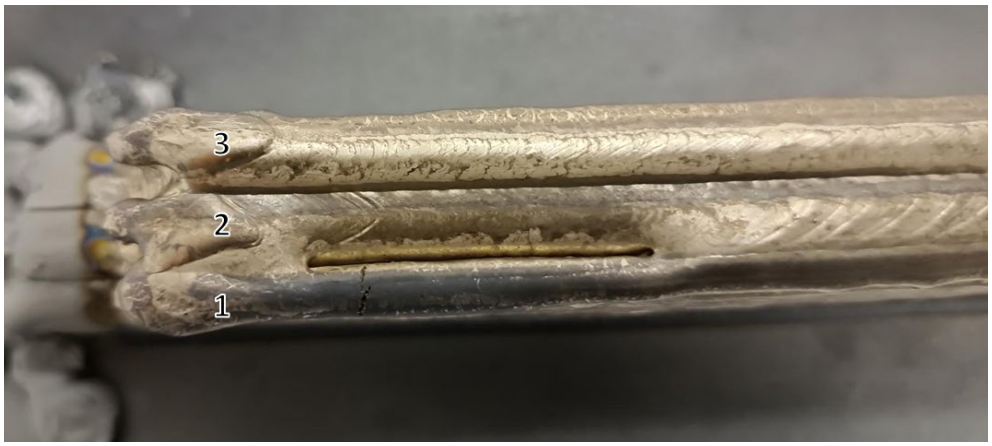

Figure 4.5: Difference in track geometry depending on inter pass temperature

Further investigation of this cracking behavior would require an additional study that is outside the scope of this project.

Figure 4.6 shows a sandblasted CuSi-3: part type 1 sample with the geometrical inhomogeneities at the track end cut off.

Figure 4.6: Sandblasted and cut CuSi-3: part type 1 sample

4.3 G3Si: part type 1

G3Si: part type 1 samples were fabricated using the procedure described in section 3.2.2 and the parameters listed in Table 11. Figure 4.7 shows a fabricated sample. G3Si does not show the same behavior of inclining at the track end, but instead displays an increased tendency to flow of the sample when the wire retraction process breaks the surface tension after deposition. This could be compensated by reducing the track length compared to the Er 316L Si part and adjusting the inter layer wait time.

Figure 4.7: Fabricated G3Si: part type 1 sample

Figure 4.8 shows a sandblasted G3Si: part type 1 sample before cutting off the sacrificial track end.

Figure 4.8: sandblasted G3Si: part type 1 sample

4.4 ER 316L Si: part type 2

ER 316L Si: part type 2 samples were fabricated using the parameters listed in Table 6. The previously observed tendency of an incline forming at the track end and of melt flowing off the sample were much more pronounced for single track walls as required for part type 2, this is visible in Figure 4.9.

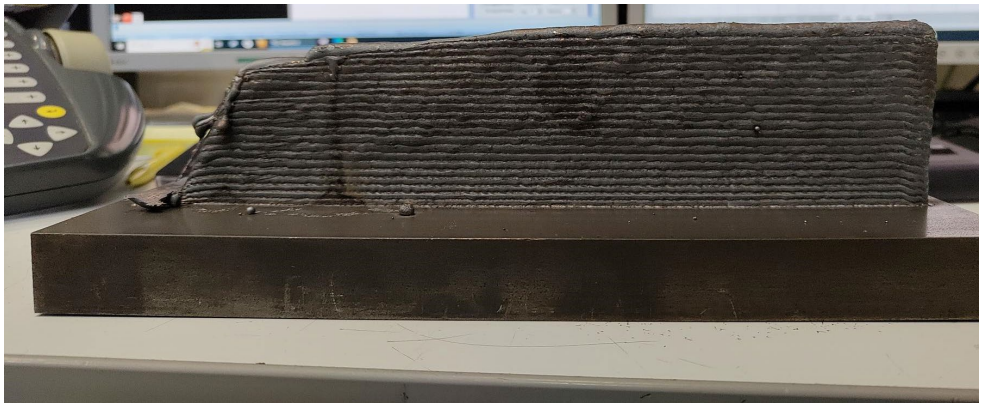

Figure 4.9: Fabricated ER 316L Si: part type 2 sample with incline and melt flow at the track end

To compensate for this behavior the track length in each consecutive layer was reduced slightly and an additional waiting time of 10 minutes between each layer was introduced. With these adaptations samples with no incline at melt flow could be fabricated as can be seen in Figure 4.10.

Figure 4.10: Fabricated ER 316L Si: part type 2 sample without incline and melt flow at the track end

4.5 CuSi-3: part type 2

CuSi-3: part type 2 samples were initially fabricated using the parameters shown in Table 10 and the procedure described in section 3.2.2. However, surface oxidation on ER 316L Si single track walls proved to be more resistant to sandblasting as can be seen in Figure 4.11.

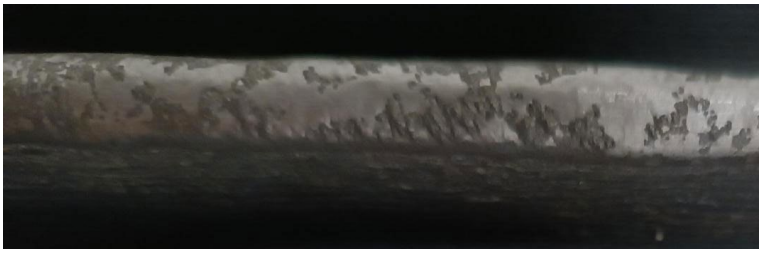

Figure 4.11: Sandblasted surface of ER 316L Si: part type 2

Therefore, the previous procedure was expanded by the following step:

- Manual removal of remaining oxides by file before deposition

Furthermore, the laser power was increased to account for a geometry dependent increase in reflection. The new parameter set is listed in Table 12.

Table 12: Parameter set for CuSi-3: part type 2

Parameter	**Value**
Laser power [W]	14200
Welding speed [mm/min]	900
Wire feed rate [mm/min]	1780
Characteristic Value	**Value**
Deposition Rate [kg/h]	7.30
Energy Density [J/mm³]	7.97

The previously observed tendency of material accumulation at the track end for CuSi-3 was even more pronounced for single track walls. In initial tests this led to an inhomogeneity in height across the track length that negatively impacted process stability. As a solution a reverse strategy from the deposition of ER 316L Si was implemented. The track length was slightly increased every two layers. The resulting overhang compensated for the excess material at the track end and a more homogenous sample geometry. Figure 4.12 shows 2 fabricated CuSi-3: part type 2 samples on the same substrate.

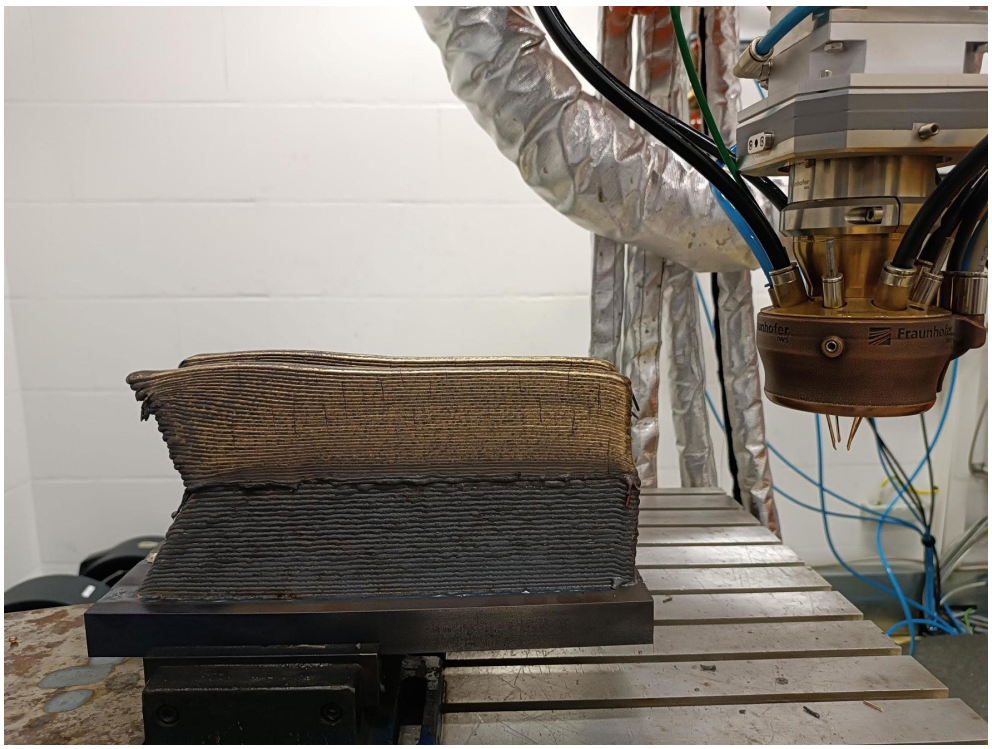

Figure 4.12: Fabricated CuSi-3: part type 2 sample

Already during production, it became clear that the problem of cracking is much more critical for single-track walls. The propagation of these cracks is similarly in build direction, perpendicular to the weld direction. However, the cracks are larger and more frequently visible at the surface. This is likely due to more uniaxial and therefore stronger internal stresses.
Most cracks occur in a distance of several centimeters from the interface. A few cracks are located very close to the interface. It is unclear whether they originated in the interface or propagated towards it. However, no surface crack propagated into the ER 316L Si.

5 Characterization of Samples

Part type 2 samples were characterized by means of light microscopy, scanning electron microscopy, energy dispersive X-ray spectroscopy and micro hardness testing with the focus on the interface region.

5.1 Characterization of CuSi-3: part type 2

Figure 5.1 shows the cross-section of CuSi-3: part type 2 by light microscopy in polished and unetched condition.

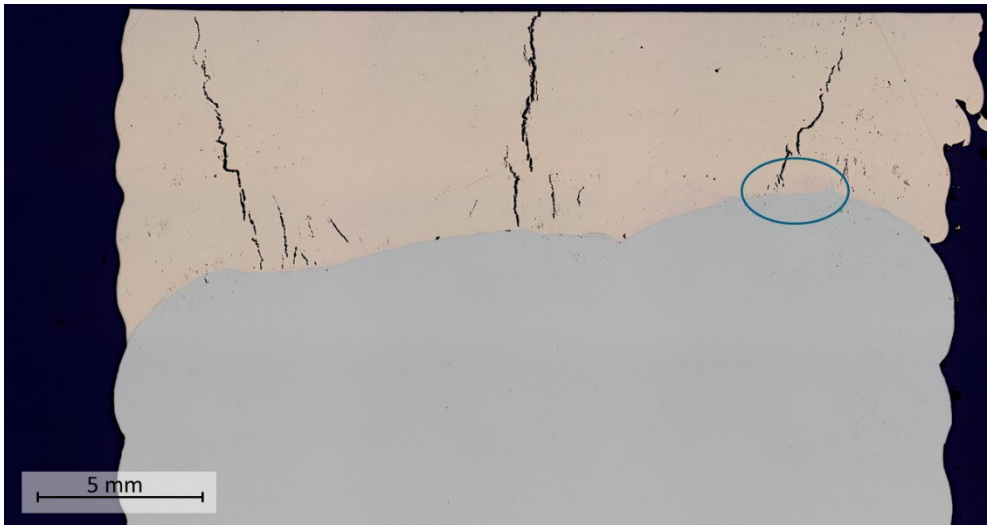

Figure 5.1: Light microscopy cross-section of CuSi-3: part type 2

The light microscopy reveals internal cracks that propagated in build direction and likely originated close to the interface. Also visible are several pores in the interface with dimensions <150 µm. However, these do not appear to function as crack origins. The CuSi-3 bulk material shows more pores with similar or smaller dimensions. The ER 316L Si material is nearly defect free with the exception of 1 pore close to the interface, all other pores are in the <15 µm range. The interface shows little dilution with the exception of some small areas like the one in the blue circle, were an unknown mix-phase is visible.

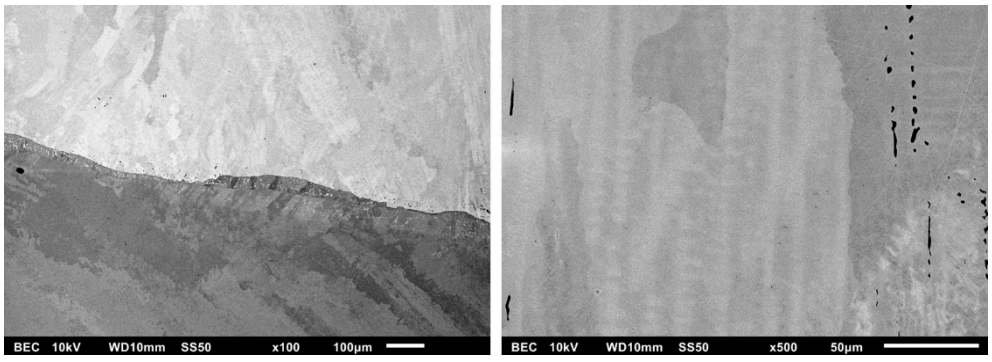

Figure 5.2: SEM imaging of cross-section of CuSi-3: part type 2. Selected areas: mix-phase (left), cracks (right).

SEM imaging (Figure 5.2, left) confirms a different microstructure in the observed mix-phase. However, the area is very small and will likely have no relevant impact on mechanical performance. The reasons for the formation of this phase, while interesting, are outside the scope of this study. The SEM imaging (Figure 5.2, right) show that at least some cracks appear to be segmented, consisting of individual pores with a strong order that aligns with the build direction.

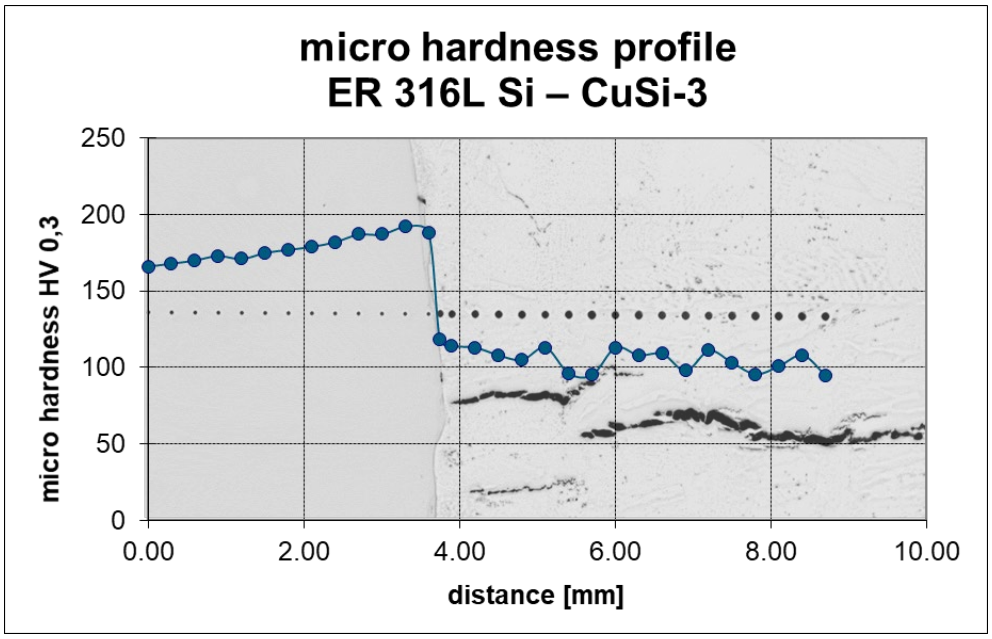

Figure 5.3: micro hardness profile of CuSi-3: part type 2

The micro hardness profile over the interface for CuSi-3: part type 2 is shown in Figure 5.3. It shows a linear increase in hardness of the ER 316L Si towards the interface. From a HV 0.3 of 166 to a maximum of 192 with a small decline to 188 closest to the interface. This is followed by a sharp drop for the CuSi-3 part to 118, followed by hardness values fluctuating between 94 and 111 with no clear trend. A slight increase in average hardness can be observed for the area 1 mm from the interface.

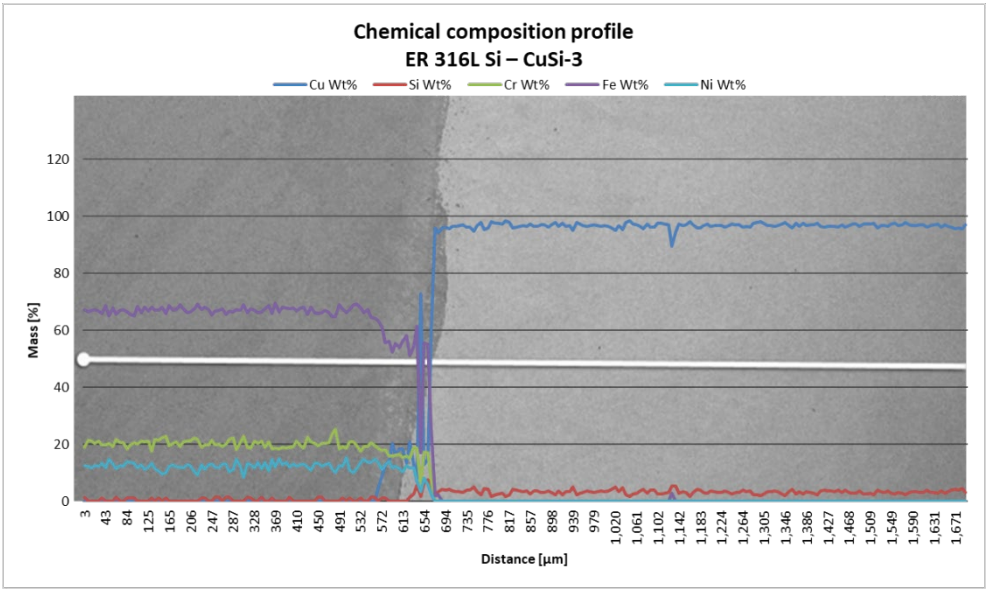

Figure 5.4: EDX: Chemical composition profile of CuSi-3: part type 2

The EDX analysis of the CuSi-3: part type 2 interface is shown in Figure 5.4. For the ER 316L Si part it shows a composition within the expected range of 20.22 % Cr and 12.35 % Ni. Other Elements, such as Si, Mn and Mo in their small mass percentages cannot be reliably detected using this method.
The chemical composition by EDX of the observed mix phase is shown more detailed in Figure 5.5.

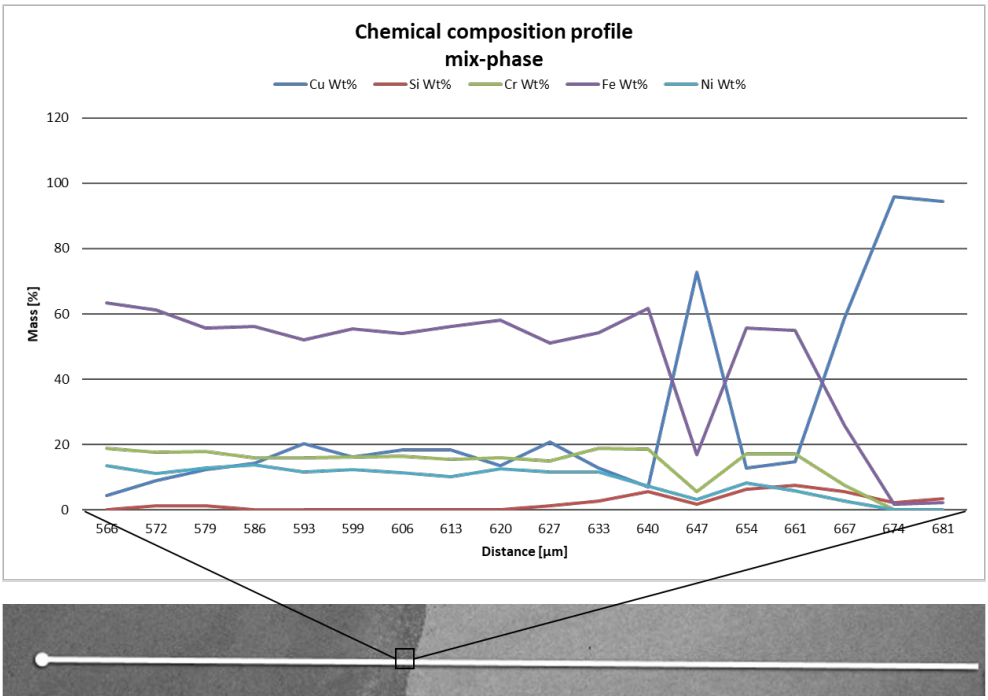

Figure 5.5: EDX: Chemical composition profile of the mix-phase

It reveals a gradual increase in Cu from 0 % for the first 30 µm with a corresponding decrease in Fe, Cr, and Ni. This is followed by ~ 50 µm of a relatively stable composition with 56.90 % Fe; 16.66 % Cr; 14.04 % Cu and 12.13 % Ni. The last 30 µm of the phase

feature strong fluctuations in Cu, Fe and Cr, with increasing amounts of Si up to 7.54%. Afterwards the Cu content continues to rise until 95.94 %.
The CuSi-3 part then displays a composition of 96.58 % Cu and 3.42 % Si on average with no detectable amount of Fe, Cr or Ni present.

This analysis confirms the presences of a localized mix-phase with a chemical composition different from the feed stock materials. However, it is very small in size comprising less than 100 µm in build direction and is not present over the entire interface.

5.2 Characterization of G3Si: part type 2

Figure 5.6 shows the cross-section of G3Si: part type 2 by light microscopy in polished and unetched condition.

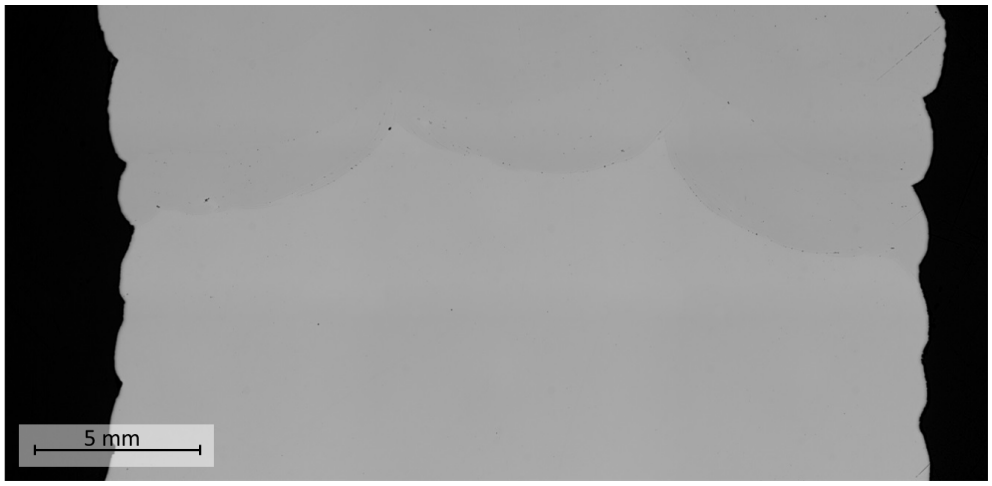

Figure 5.6: Light microscopy cross-section of G3Si: part type 2

It shows that the ER 316L Si material is again nearly defect free with only micro porosity in the <15 µm range. Some larger pores <150 µm are visible in the interface region. The G3Si bulk material is also nearly defect free with no porosity >15 µm or cracks. The scratch visible in the top right corner is most likely due to metallographic preparation. Notably the G3Si shows significantly increased penetration into the Er 316L Si compared to CuSi-3.

Figure 5.7 shows a section of the same sample but after etching with Nital 2%.

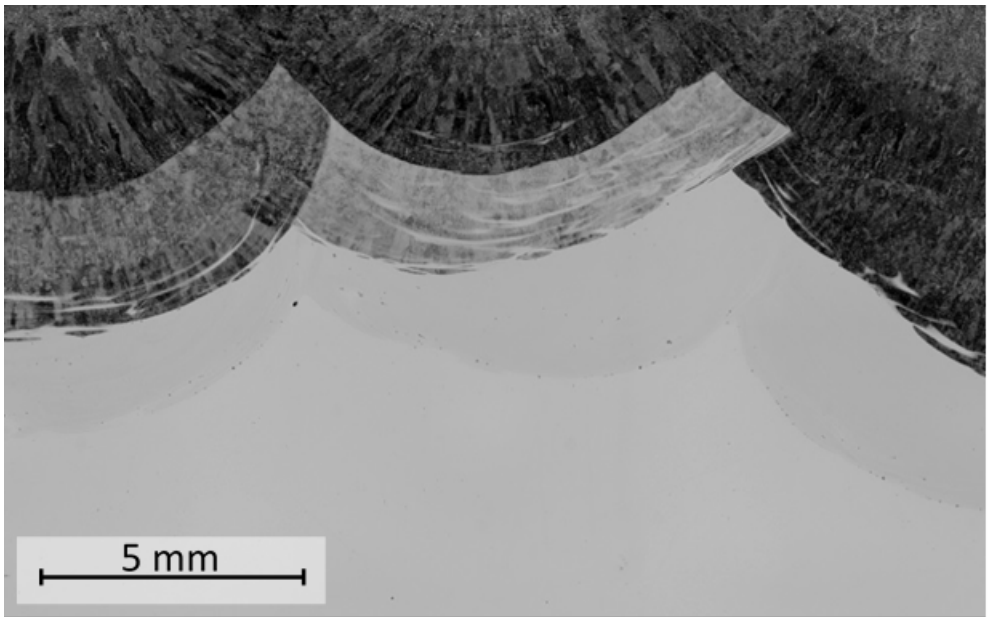

Figure 5.7: Etched light microscopy cross-section of G3Si: part type 2

A strongly selective attack of the etching agent is visible. The ER 316L Si material shows is nearly unaffected by the etching. For the G3Si part individual tracks are clearly visible and etched to varying degrees. This suggests substantial dilution especially in the interface layer, but also partly in the second layer.

Figure 5.8 shows the microstructure of ER 316L Si and G3Si by SEM imaging.

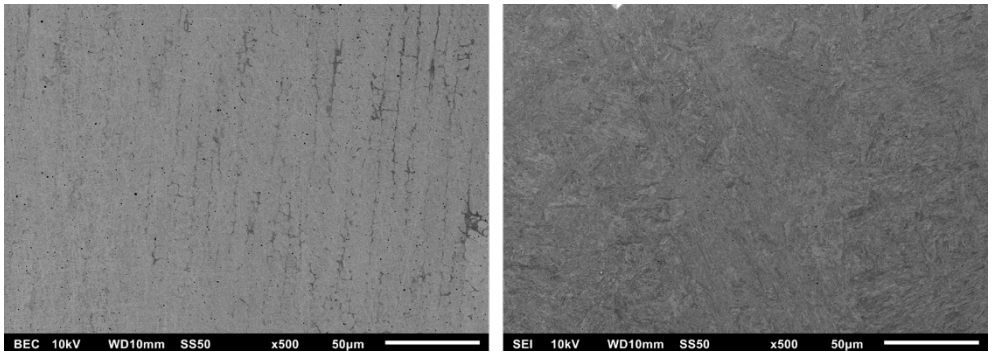

Figure 5.8: SEM imaging: microstructure of ER 316L Si (left) and G3Si (right)

The previously observed micro porosity is confirmed in the SEM of ER 316L Si. The microstructure is likely a gamma austenite matrix with a directional grown delta ferrite network. The microstructure of G3Si is completely different with no clear preferred growth direction and seemingly much finer needle like grains. Specific phases could not be identified but likely include alpha ferrite, perlite, tertiary cementite and potentially austenite. Figure 5.9 shows the microstructure in the interface and reveals a sharp border between the microstructures with almost no transition zone. The G3Si part appear to show slightly less micro-porosity compared to Er 316L Si.

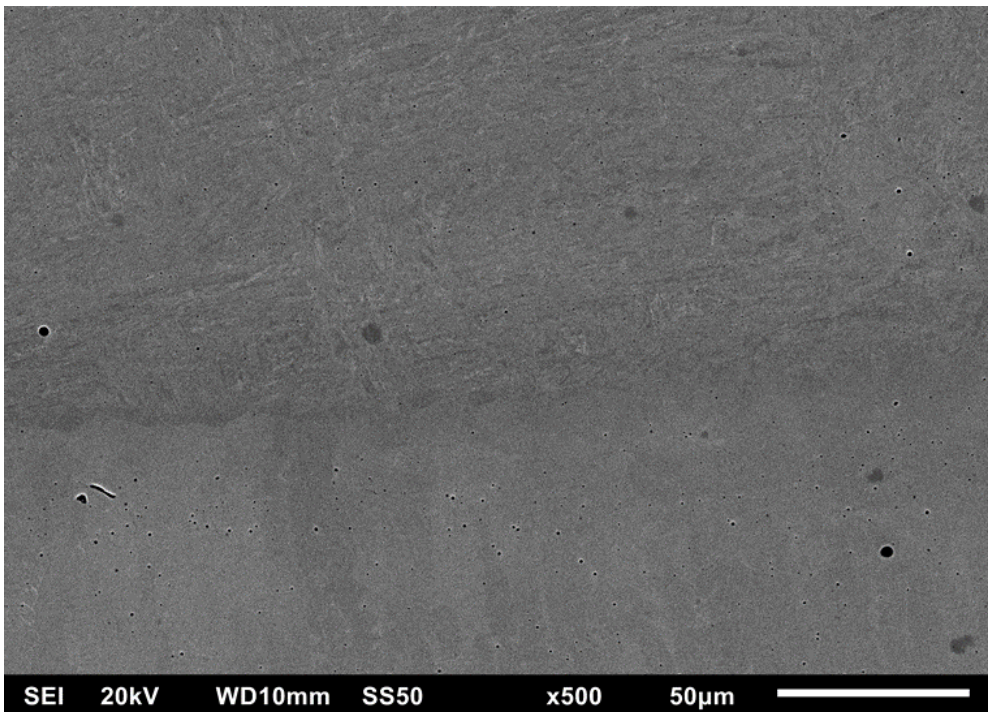

Figure 5.9: SEM imaging: microstructure of the ER 316L Si (down) – G3Si (up) interface

Figure 5.10 shows the micro hardness profile over the ER 316L Si – G3Si interface.

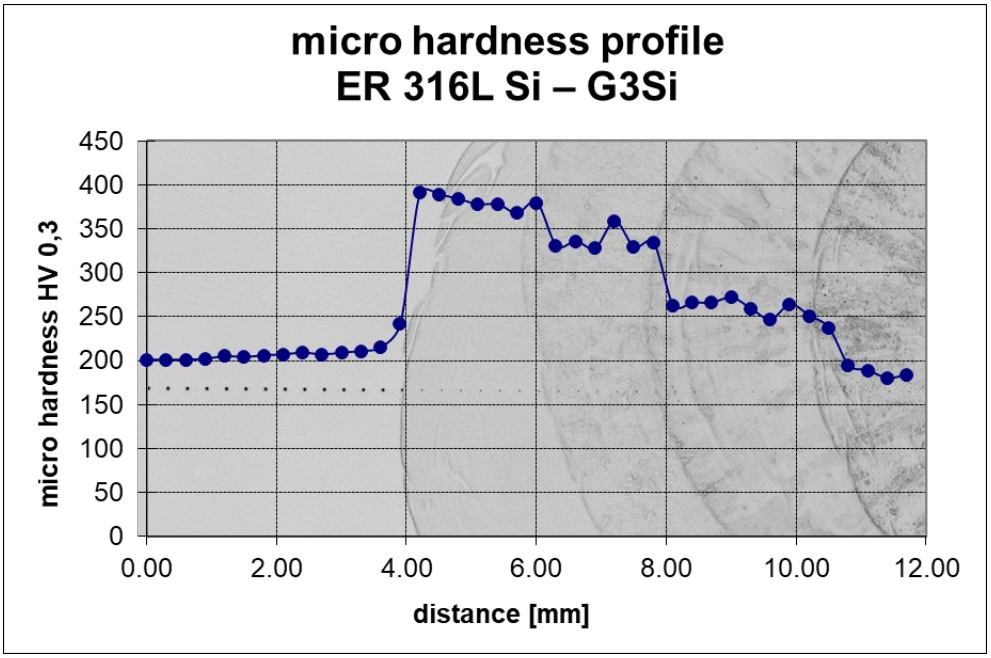

Figure 5.10: micro hardness profile of G3Si: part type 2

In the ER 316L Si a slight increase in hardness from 201 to 242 HV 0.3 towards the interface is observed. This is followed by a sharp increase for the first G3Si layer to 391 HV 0.3 with the average hardness of the layer being 381.14 HV 0.3. The next two layers also show increased micro hardness with 336.17 and 261.00 HV 0.3 respectively. The fourth layer still shows 237 HV 0.3 close to the layer interface but then decreases to an average HV 0.3 of 187.00.

Figure 5.11 shows the chemical composition profile of the ER 316L Si – G3Si interface by EDX over the interface.

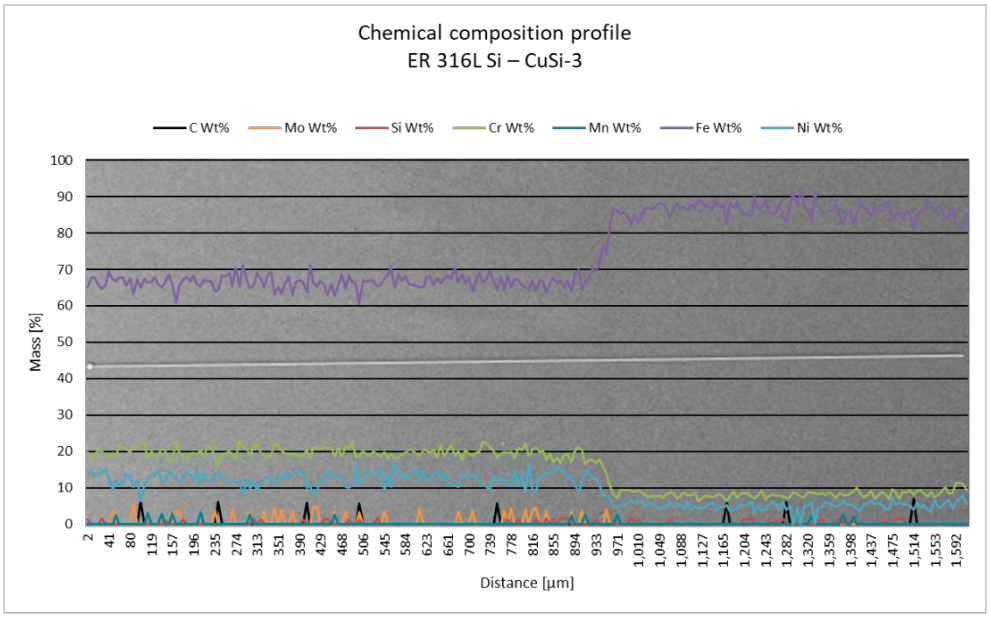

Figure 5.11: EDX: Chemical composition profile of G3Si: part type 2

The average chemical composition of the first ~900 µm in the Er 316L Si part is as follows: 66.53 % Fe; 19.69% Cr and 12.42% Ni with the other elements being detected occasionally as they are at the threshold of detectability. The composition then gradually changes over a distance of ~50 µm to an average composition of 86.21 % Fe; 8.27% Cr and 4.99 % Ni with occasional detections of Si, C and Mn. Mo was never detected in the G3Si-part.
This confirms substantial dilution of the first G3Si layer with a different composition to the feedstock material. Further EDX investigations of the interface to the second layer have shown a reduction of the Cr content to ~5 % with Ni being only sometimes detectable.